Soft Matter

Dynamic Article Links

Cite this: *Soft Matter*, 2011, **7**, 8961

www.rsc.org/softmatter

PAPER

Environment effect on the redox properties of Self-Assembled Monolayers: a theoretical investigation of the nature of the supporting electrolyte

Gaëlle Filippini, Florent Goujon, Christine Bonal* and Patrice Malfreyt

Received 22nd April 2011, Accepted 9th June 2011
DOI: 10.1039/c1sm05738c

Gibbs free energy calculations have been performed to calculate the change in the simulated redox properties of FcC_6S–/$C_{12}S$–Au and FcC_6S–/C_4S–Au in three different electrolytes ($NaClO_4$, Na_2SO_4 and $NaPF_6$). The effect of surface ion association between the ferricinium cation and the electrolyte anions is investigated on the redox properties of SAMs. The microscopic description of the binary SAMs before and after oxidation indicates that the formation of surface ion pairs is strongly correlated with the hydration energy of the corresponding anion. The correlation between the desolvation of the anions and the ion-pairs formation is established. We have shown from the energy contributions that a general understanding of the thermodynamic behavior of these systems should be analyzed in the context of the enthalpy–entropy compensation effect.

1. Introduction

A ferrocene-terminated alkanethiol system is the most representative example of an electroactive Self-Assembled Monolayer (SAM).[1–7] They carry not only a fundamental interest, but they have also attracted much interest in recent years for their numerous applications in sensors and molecular electronic devices.[8–12] The redox behaviors of these SAMs have been well-studied by cyclic voltammetry.[13–22] In fact, considerable efforts have been made to explore the relationships between molecular structures, surfaces and surface properties.[2,3,5,16,22–24] One of the most noticeable features of the Fc-terminated SAMs is the sensitivity of their electrochemical properties to a variety of surface and solution parameters. These parameters include coverage, orientation, chain lengths of the alkanethiol and the electrolyte system.

MD simulations have been shown to be highly successful in capturing both the structural and energetic properties of SAMs.[25–29] Recently, we have demonstrated that molecular simulation can be used to obtain quantitative informations to establish connections between electrochemical experiments and MD simulations.[29] In a previous paper, we studied two systems: a binary SAM formed by ferrocenylhexanethiol and coadsorbed dodecanethiol (FcC_6S–/$C_{12}S$–Au) and another binary SAM composed of ferrocenylhexanethiol and coadsorbed butanethiol (FcC_6S–/C_4S–Au). We have demonstrated that the free energy perturbation methods are able to reproduce the change in the redox potential in electroactive SAMs as the environment of the ferrocene moiety is modified. This work allows us to consider the free energy formalism as an efficient tool for the prediction of the redox properties of SAMs. The replacement of the coadsorbed butanethiolate by dodecanethiolate chains induces a positive shift of the redox potential. This shift is due to the partial immersion of the redox center in the hydrocarbon layer. This environment stabilizes ferrocene to a greater extent than for ferricinium. This is well reproduced by the free energy calculations. Interestingly, our results have also highlighted the formation of an ion-pair between a single perchlorate anion of the supporting electrolyte and the ferricinium ion.

As already mentioned above, it is well known that the redox potentials of the surface confined molecules on gold in contact with an electrolyte solution are significantly affected by the type of electrolytes in solution. More precisely, the nature and the concentration of anions in the electrolyte are evidenced to affect the position and the shape of the redox waves obtained by cyclic voltametry[3,8,13,14,22,30,31] and the stability of the SAM upon repeated potential cycling in aqueous solution.[30,31] While the oxidation wave of the ferrocenyl group in $HClO_4$ solution is fairly sharp and reversible, the response is rather irreversible and the redox peaks shift positively[13,14] in H_2SO_4 solution. The difference is mainly interpreted in terms of the different stability of the ion-pair between the one-electron-oxidized ferrocenyl moiety (total charge increases from 0 to +1) and the electrolyte anions.

In this paper we focus on the influence of electrolyte solutions to investigate how the fact that the ferrocenium cation (Fc^+) forms ion pairs might be related to the stability and other physical and chemical properties of Fc-terminated monolayers. Our purpose is to understand in detail the role of the electrolyte in redox processes. More precisely, our methodology using perturbation methods is extended to obtain the change in the simulated redox properties of the two systems previously studied

Clermont Université, Université Blaise Pascal, Laboratoire de Thermodynamique et Interactions Moléculaires, CNRS, UMR 6272, LTIM, BP 10448, F-63000 CLERMONT-FERRAND. E-mail: Christine.Bonal@univ-bpclermont.fr; Fax: +33 473 40 53 28; Tel: +33 473407165

(FcC_6S–/$C_{12}S$–Au and FcC_6S–/C_4S–Au) as a function of the following electrolyte solutions (*e.g.*, $NaClO_4$, Na_2SO_4, $NaPF_6$). The fact that the electrochemical signatures of these systems with anion species, such as ClO_4^- and SO_4^{2-}, are known, offers direct comparison with our own calculations.[22] We have also explored the influence of PF_6^- using MD simulations as a predictive tool. This work is completed with a microscopic description associated with an energy characterization of these SAMs as a function of the electrolyte anions.

In the present paper, we aim at addressing the following questions: do the free energy perturbation methods reproduce the small difference in the redox properties as a function of the electrolyte anion? How does the nature of the anion impact on the thermodynamic properties of the interfacial redox reactions? Is there a correlation between the shift in the free energies, the $\Delta\Delta G$ and the strength of the ion pair? Is it possible to make a link between the anion's ability to ion pair and the hydration energy of the anion in solution?

The outline of the paper is as follows. In Section 2, we present the computational procedures and give the simulation details. The results are discussed in Section 3. Finally, we conclude in Section 4 providing a brief summary of our main results.

2. Computational procedures

2.1 Model

The system consists of five layers of an Au(111) surface grafted with either *n*-C_4 alkylthiol (C_4H_9S) or *n*-C_{12} alkylthiol ($C_{12}H_{25}S$) molecules and one FcC_6S ferrocenylhexanethiol ($C_{16}H_{21}FeS$). We used the all-atom (AA) version of the Cornell force field AMBER[32] for grafted molecules. The general potential function is of the form

$$U = U_{\text{bond}} + U_{\text{angle}} + U_{\text{dihedral}} + U_{\text{LJ}} + U_{\text{ele}} \quad (1)$$

where

$$U_{\text{bond}} = \sum_{\text{bonds}} \frac{1}{2} k_{\text{b}} (r - r_{\text{o}})^2 \quad (2)$$

$$U_{\text{angle}} = \sum_{\text{angles}} \frac{1}{2} k_{\theta} (\theta - \theta_{\text{o}})^2 \quad (3)$$

$$U_{\text{dihedral}} = \sum_{\text{dihedrals}} k_{\phi} [1 + \cos(l\phi + \delta)] \quad (4)$$

$$U_{\text{LJ}} = \sum_{i=1}^{N-1} \sum_{j>i}^{N} 4\varepsilon_{ij} \left[\left(\frac{\sigma_{ij}}{r_{ij}} \right)^{12} - \left(\frac{\sigma_{ij}}{r_{ij}} \right)^{6} \right] \quad (5)$$

where k_{b}, k_{θ} and k_{ϕ} are the force constants for deformation of bonds, angles and dihedrals, respectively. The equilibrium values of bond distances and valence angles correspond to r_{o} and θ_{o}, respectively. In the dihedral angle term, l is the periodicity and δ is the phase factor. The C–H covalent bonds were kept of fixed length by using the SHAKE algorithm.[33] The intermolecular and intramolecular interactions due to the repulsion–dispersion interactions are calculated using the Lennard-Jones (LJ) potential, represented by eqn (5). In the AMBER force field, the nonbonded interactions between atoms separated by exactly three bonds (1–4 LJ interactions) are reduced by a factor of 0.5.[32] The Lennard-Jones potential parameters for the interactions between unlike atoms were calculated by using the Lorentz–Berthelot mixing rules (quadratic and arithmetic rules for ε_{ij} and σ_{ij} parameters, respectively). The water molecules were represented by the TIP4P/2005 model.[34] As the system is non-periodic in the direction normal to the surface (z-axis), the simulation cell is closed by an additional gold layer. The distance between the two inner surfaces was chosen to be 80 Å, which is large enough for the water molecules in the middle of the cell to have bulk behavior.[27] To investigate the effect of the supporting electrolyte, simulations were performed in $NaClO_4$, $NaPF_6$ and Na_2SO_4 aqueous solutions. The Na^+ parameters were taken from Aqvist forcefield.[35] ClO_4^- ions are represented using the model described by Wu *et al.*[36] PF_6^- ions' parameters were determined by Kaminski *et al.*[37] SO_4^{2-} ions were modeled with parameters published by Cannon *et al.*[38]

2.2 Electrostatic interactions

The last term in eqn (1) corresponds to the electrostatic energy (U_{ele}) of the system. The electrostatic interactions are calculated with the Smooth Particle Mesh Ewald (SPME) method.[39] For a neutral periodic system with orthogonal axis, the electrostatic potential U_{ele} is defined as

$$U_{\text{ele}} = U_{\text{R}} + U_{\text{K}} + U_{\text{self}} + U_{\text{excl}} + U_{M_z} \quad (6)$$

$$U_{\text{R}} = \frac{1}{8\pi\varepsilon_o} \sum_i \sum_a \sum_{j \neq i} \sum_b q_{ia} q_{jb} \frac{\text{erfc}\ (\alpha r_{iajb})}{r_{iajb}} \quad (7)$$

where the sums are over all atoms a in molecule i and all atoms b in molecule j. r_{iajb} is the distance between the atoms a and b belonging to two different molecules i and j and q_{ia} and q_{jb} represent the charges on atoms a and b, respectively. This term is pairwise-additive and short-ranged and a spherical cutoff can be used with periodic boundary conditions. α is chosen so that only atom–atom pair interactions between different molecules in the central cell ($n = 0$) need to be considered. erf(x) is the error function whereas erfc(x) is the complementary error function. Note that the overall charge of the simulation box must be zero.

The reciprocal space part U_{K} of the potential is expressed as

$$U_{\text{K}} = \frac{1}{2V\varepsilon_o} \sum_{k \neq 0} \frac{1}{k^2} \exp\left(-\frac{k^2}{4\alpha^2} \right) \left| \sum_i \sum_a q_{ia} \exp(-i\, \mathbf{k}.\mathbf{r}_{ia}) \right|^2 \quad (8)$$

where V is the simulation cell volume, r_{ia} is the cartesian coordinate of site a in molecule i. The reciprocal lattice vector $\mathbf{k}$ are defined as $\mathbf{k} = 2\pi(l/L_x\mathbf{u},\ m/L_y\mathbf{v},\ n/L_z\mathbf{w})$ where $\mathbf{u}$, $\mathbf{v}$, $\mathbf{w}$ are the reciprocal space basis vectors and l, m, n take values of 0, ±1, ±2,··· ±∞. The reciprocal space sum is truncated at an ellipsoidal boundary at the vector $|\mathbf{k}^{max}|$. This term includes all the intramolecular interactions due to the bonded atoms.

The U_{excl} term is added to correct for the contributions due to intramolecular electrostatic interactions. It is expressed as

$$U_{\text{excl}} = -\frac{1}{8\pi\varepsilon_o} \sum_i \sum_a \sum_{b \neq a} q_{ia} q_{ib} \frac{\text{erf}(\alpha r_{iaib})}{r_{iaib}} \quad (9)$$

where the sums are over atoms bonded to atoms a and b of the same molecule i through bonds, valence and dihedral potentials.

A fourth correction U_{self} term is required to correct for the fact that the sum of Gaussian functions in the real space includes the interactions of each Gaussian with itself.

$$U_{\text{self}} = -\frac{\alpha}{4\pi^{3/2}\varepsilon_o}\sum_i \sum_a q_{ia}^2 \quad (10)$$

A fifth term, U_{M_z}, is included to consider the supercell approximation[40] and is defined as

$$U_{M_z} = \frac{1}{2\varepsilon_o V} M_z^2 \quad (11)$$

where M_z is the net dipole moment of the simulation cell given by $\sum_{i=1}^{N} q_i \mathbf{r}_i$. This contribution is the correction term of Yeh and Berkowitz,[40] which results from the plane-wise summation method proposed by Smith.[41] Adding this term to the total energy implies the use of a z-component force for each atom given by

$$F_{i,z} = -\frac{q_i}{\varepsilon_o V} M_z \quad (12)$$

The supercell approximation[40] consists of elongating the z-dimension of the simulation cell by placing an empty space of at least four times the space of the fluid-occupied region. The use of this approximation and the dipole correction allow to apply the conventional three-dimensional SPME technique to the calculation of the electrostatic interactions in a slab geometry.[27]

2.3 Free energy calculations

The differences in Helmholtz free energies between states (0) and (1) of a same molecular system were calculated using the Thermodynamic Integration (TI) method. The TI and FDTI (Finite Difference Thermodynamic Integration) methods were found to give comparable results on our systems.[29]

The perturbation process is performed between states (0) and (1) in the constant-NVT ensemble using a "double wide sampling" over N_w intermediate contiguous windows defined by the coupling constant λ. The TI method expresses the change in Helmholtz free energy as the following integral

$$\Delta A_{\text{TI}} = \int_0^1 \left\langle \frac{\partial U(r,\lambda)}{\partial \lambda} \right\rangle_\lambda \mathrm{d}\lambda \quad (13)$$

where the derivative of $U(r, \lambda)$ with respect to λ can be calculated using a central finite difference technique between $U(r, \lambda + \delta\lambda)$ and $U(r, \lambda - \delta\lambda)$

$$\left\langle \frac{\partial U(r,\lambda)}{\partial \lambda} \right\rangle_{\lambda,\text{CD}} = \left\langle \frac{(U(r,\lambda+\delta\lambda) - U(r,\lambda-\delta\lambda)}{2\delta\lambda} \right\rangle_\lambda \quad (14)$$

$\delta\lambda$ is taken to be sufficiently small ($\delta\lambda = 0.0001$) to avoid hysteresis between calculations carried out from state λ to state $\lambda + \delta\lambda$ and from state λ to state $\lambda - \delta\lambda$. The integration over λ is carried out by a trapezoidal algorithm.

As shown previously,[29] the Helmholtz free energy change (ΔA) can be assimilated to Gibbs free energy change (ΔG).

The entropy change ΔS[42] calculated using the TI approach is given by

$$\Delta S = \frac{1}{kT^2}\int_0^1 \left[\langle U(r,\lambda)\rangle_\lambda \left\langle \frac{\partial U(r,\lambda)}{\partial \lambda} \right\rangle_\lambda - \left\langle \frac{\partial U(r,\lambda)}{\partial \lambda} U(r,\lambda) \right\rangle_\lambda \right] \mathrm{d}\lambda \quad (15)$$

2.4 Simulation details

The gold surface is composed of five (111) layers of a 9×10 fcc lattice, so that the dimensions of the simulation box along the x and y axes are 25.9 Å and 24.9 Å, respectively. One ferrocenylhexanethiolate (FcC_6S) chain is grafted onto the surface with an initial tilt angle $\theta = 30°$. The remaining space is filled by grafting either 27 C_4S or 27 $C_{12}S$ alkylthiolate chains, using a minimal distance between grafting points corresponding to an experimental surface coverage of 1/3. This results in a ferrocene surface coverage of 2.5×10^{-11}mol cm^{-2} (5% of a full monolayer) in line with the corresponding experimental coverage.[22] The simulation cell is closed by an additional gold layer formed by 90 gold atoms. The separation distance between the two surfaces is fixed to 80 Å. The simulation cell is then elongated in the positive and negative z-directions with vacuum space to yield a L_z dimension of 447 Å.

Two systems A and B are considered. System A is a FcC_6S–/C_4S–Au SAM and system B is a FcC_6S–/$C_{12}S$–Au SAM. Both systems are described in Table 1. Simulations are performed with three different supporting electrolytes, sodium perchlorate ($NaClO_4$), sodium hexafluorophosphate ($NaPF_6$) and sodium sulfate (Na_2SO_4). The water molecules and the cations and anions of the supporting electrolyte are randomly added in the remaining volume in order to respect a concentration of 1 M for the electrolyte in line with the experimental conditions.[22]

Simulations are run in the constant-NVT statistical ensemble using a Nose–Hoover thermostat[43] with a coupling constant of 0.5 ps. The equations of motion are integrated using the Verlet leapfrog algorithm scheme at $T = 298$ K with a timestep equal to 2 fs. The cutoff radius for the Lennard-Jones and the real space of the electrostatic interactions is fixed to 12 Å. The Ewald convergence parameter α is fixed to 0.2651 Å^{-1}. The maximum reciprocal lattice vectors parallel to the gold surfaces are given by $k_x^{\max} = k_y^{\max} = 8$. As the simulation cell is elongated along z, $k_z^{\max}$ is increased up to 128. This price must be paid to use the standard three dimensional Ewald summation in a slab geometry and to account accurately for the long-range electrostatic interactions. With these parameters, the calculation of the electrostatic interactions using the Smooth Particle Mesh Ewald method yields a relative error of 10^{-6}. The configurations are generated using the parallel version of the modified DL_POLY_MD package[44] by using up to 8 processors at a time. A typical NVT simulation run consists of an equilibrium period of 500 ps and an additional acquisition phase of 400 ps.

The oxidation of the ferrocene moiety in the ferrocenylalkylthiolate chain in the A and B systems is carried out by using a perturbation process. It consists of changing the charge of the ferrocene moiety from 0.0 ($\lambda = 0.0$) to 1.0 ($\lambda = 1.0$). The partial charges of the ferrocene group are taken from the force field

Table 1 Number of molecules in the simulation cell for A and B

molecule type	A FcC_6S–/C_4S–Au	B FcC_6S–/$C_{12}S$–Au
C_nS	27	27
FcC_6S	1	1
water	1514	1319
electrolyte	27	24

developed by Canongia *et al.*[45] The partial charges of the ferricinium group have been calculated from density-functional theory (DFT)[46,47] (B3LYP)[48–50] with effective core potential (SDDALL) Gaussian basis using the Gaussian 03 package[51] and the CHELPG[52] procedure as a grid-based method. The perturbation of the partial charges affects all the atoms of the ferrocene group and the last three methylene groups of the alkyl chain bound to ferrocene through bonds, valence and dihedral angle potentials. In order to respect the electroneutrality of the system, a sodium cation vanishes between $\lambda = 0.0$ and $\lambda = 1.0$. This cation is frozen at a sufficiently large distance ($z = 76$ Å) in order not to interfere with the monolayer. The perturbation is carried over 11 contiguous states or windows defined by the coupling parameter λ. The variations of the potential energy $U(r, \lambda)$ during the mutation of the sodium cation were calculated using a linear combination of the LJ parameters (σ, ε) of the initial state (0) ($\lambda = 0.0$) and final state (1) ($\lambda = 1.0$) using the following mixing rules:

$$\varepsilon_{ij}(\lambda) = \lambda\left(\sqrt{(\varepsilon_{ii}(1)\varepsilon_{jj})}\right) + (1-\lambda)\left(\sqrt{(\varepsilon_{ii}(0)\varepsilon_{jj})}\right) \quad (16)$$

$$\sigma_{ij}(\lambda) = \lambda\left(\frac{\sigma_{ii}(1)+\sigma_{jj}}{2}\right) + (1-\lambda)\left(\frac{\sigma_{ii}(0)+\sigma_{jj}}{2}\right) \quad (17)$$

where i and j represent perturbed and unperturbed atom types, respectively. The atomic site charge q is also expressed as a function of λ as follows

$$q_i(\lambda) = \lambda q_i(1) + (1-\lambda) q_i(0) \quad (18)$$

where i represents the perturbed atomic site. The values of the partial charges for the ferrocene and methylene groups and the Lennard-Jones parameters for the sodium cations are given for completeness in Table 7 and in Fig. 7 for the initial and final states. The total simulation for completing the perturbation calculation over 11 windows is about 10 ns.

3. Results and discussions

3.1 Determination of $\Delta\Delta G^{cal}_{redox}$

We have shown in previous studies[29] that the redox reactions represented in Fig. 1 allow us to compare the difference in the calculated free energies $\Delta\Delta G$ with the experimental results. This difference in the calculated free energies is obtained from $\Delta\Delta G = \Delta G_B - \Delta G_A$ where A refers to FcC_6S–C_4S–Au SAM and B refers to FcC_6S–$C_{12}S$–Au SAM.

As we model the oxidative reactions, the computed free energies are of opposite sign compared to the experimental free energies that correspond to reductive processes. We report in Table 2 the values of $\Delta\Delta G^{cal}_{redox}$ obtained from perturbation methods for three different electrolytes:$NaClO_4$, $NaPF_6$ and Na_2SO_4. The calculated $\Delta\Delta G^{cal}_{redox}$ redox property can be assimilated to $-nF\Delta\Delta E^{\circ\prime}$ where F is Faraday's constant and n is equal to 1. The $\Delta\Delta E^{\circ\prime}$ corresponds to the shift in redox potential when the alkanethiol coadsorbate length increases from 4 to 12. As one can see in Table 2, we find excellent agreement between the simulated and available experimental redox properties. We note that the $\Delta\Delta G^{cal}_{redox}$ values increase in the order $ClO_4^- < PF_6^- < SO_4^{2-}$. At this stage, the interpretation of the shift in the $\Delta\Delta G^{cal}_{redox}$ as a function of the anion is not straightforward because it involves a difference between the Gibbs free energy of a redox reaction in the two systems A and B. Thus, we must focus on the molecular description and energetic properties of these monolayers for a deeper interpretation of the trends observed in the $\Delta\Delta G^{cal}_{redox}$ values.

$$(Fc^+)_A + e^- \xrightarrow{\Delta G_A} (Fc)_A$$

$$(Fc^+)_B + e^- \xrightarrow{\Delta G_B} (Fc)_B$$

Fig. 1 Redox reactions used to model the effect of the environment on the change in the redox properties of FcC_6S–C_4S–Au (System A represented by $(Fc)_A$) and FcC_6S–$C_{12}S$–Au (System B represented by $(Fc)_B$) SAMs.

3.2 Ion pair formation

We now focus on the microscopic description of the binary SAMs in the initial ($\lambda = 0.0$) and final ($\lambda = 1.0$) states as a function of the electrolyte anions. The molecular density profiles of coadsorbed C_4S butanethiol chains, FcC_6S ferrocenylhexanethiol chain and supporting anions along the z direction are represented in Fig. 2. The initial state with the ferrocene headgroup is represented in panel a) whereas panel b) shows the density profiles in the final state where the ferrocene is oxidized. Panel c) and d) report the same profiles with coadsorbed $C_{12}S$ dodecanethiol chains.

For $\lambda = 1.0$, we observe that the density profiles of ClO_4^- and PF_6^- (panels b and d) are significantly changed in the two systems. In fact, they are shifted toward the ferrocenium group indicating that these anions interact further with the ferrocenium cation. We do not observe any change in the density profiles of SO_4^{2-} ions for both systems A and B. This shows the lesser tendency of this anion in forming ion pairs.

In order to further investigate the ion-pairing tendencies, we have calculated the mean distances between the ferrocene moities and the center of mass of the closest anion before and after the oxidation. Values are included in Table 3 for the two SAM systems as a function of the electrolyte anion. The poorest ion-pairing ability of SO_4^{2-} in A and B is confirmed by the largest $SO_4^{2-} \cdots Fc^+$ distance (9 and 14 Å, respectively). The energy contributions between these two ions are then very weak: −5 and 0 kJ mol^{-1} for A and B, respectively.

By contrast, we observe a shorter distance $PF_6^- \cdots Fc^+$ in A and B (see Table 3). The energy contribution of this ion-pair is then −22 kJ mol^{-1} in A against −37 kJ mol^{-1} in B. The same trend is obtained with ClO_4^-. The energy contributions between $ClO_4^- \cdots Fc^+$ is about −17 kJ mol^{-1} in A and −46 kJ mol^{-1} in B. We observe that these ion-pairs are always stronger in B than in A: the energy contributions are much favored with smaller average distances between the two ions. This is in line with previous

Table 2 Differences in the free energy contributions $\Delta\Delta G^{calc}_{redox}$ (kJ mol^{-1}) as a function of the electrolyte anion along with the experimental redox property $\Delta\Delta E^{exp}_{redox}$ values (V).[22]

	$-\Delta\Delta G^{calc}_{redox}$	$-\Delta\Delta E^{calc}_{redox}$	$\Delta\Delta E^{exp}_{redox}$
ClO_4^-	21	0.22	0.19
PF_6^-	23	0.24	
SO_4^{2-}	26	0.27	0.29

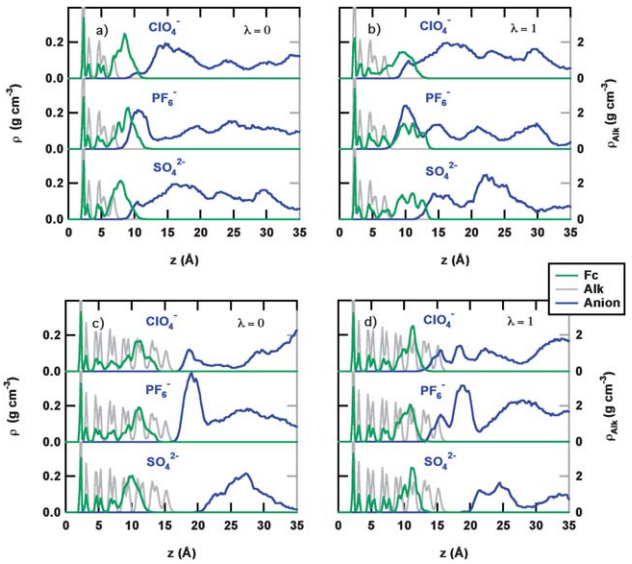

Fig. 2 Molecular density profiles of the coadsorbed butanethiolate chains, ferrocenylhexanethiolate chain, and counterions as a function of the electrolyte anions for (a) $\lambda = 0.0$ and (b) $\lambda = 1.0$. The same profiles are given in panels (c) and (d) where the dodecanethiolate chains replace the coadsorbed butanethiolate chains.

conclusions[29] demonstrating that the formation of the ion-pair is more favored in SAMs with longer alkyl chains when the environment of the ferrocenium becomes more alkane-like. In summary, all these results clearly demonstrate that the ion pairing stabilizes the electrogenerated cation. Typical configurations of the tight complexation to the SAM-bound ferrocenium of PF_6^- in system A and of ClO_4^- in system B are shown in panels a) and c) of Fig. 3 for illustration. In panels b) and d) of Fig. 3, we have also reported a typical configuration showing the absence of ion pairing in both systems A and B with SO_4^{2-}.

We now turn to the distributions of the distance between the ferrocene group and the closest electrolyte anion for different electrolyte anions. Fig. 4 depicts the results obtained for system B at $\lambda = 0.0$ and $\lambda = 1.0$. We focus on B because of the higher pairing tendency in longest coadsorbed chains. Before oxidation, a broad peak is observed for each electrolyte anion. The peaks for ClO_4^- and PF_6^- anions are located at the same position whereas a distribution at higher distance is observed for SO_4^{2-}. After oxidation, the emergence of a well-defined peak for ClO_4^- and PF_6^- anions is observed reflecting thus a higher ordering within the structure. This can be easily explained by the penetration of the anions into the film to form tightly ions-pairs to the ferrocenium. This underlines that both enthalpic and entropic factors must be considered to fully describe these systems. Note that when the length of the alkyl chain of the coadsorbate is

Table 3 Distances (Å) between ferrocenium cation and the closest electrolyte anion in A and B at $\lambda = 0.0$ and $\lambda = 1.0$

	A		B	
	$\lambda = 0$	$\lambda = 1$	$\lambda = 0$	$\lambda = 1$
ClO_4^-	7.0	6.8	12.8	4.9
PF_6^-	6.8	5.7	12.1	5.3
SO_4^{2-}	14.3	9.0	16.1	14.0

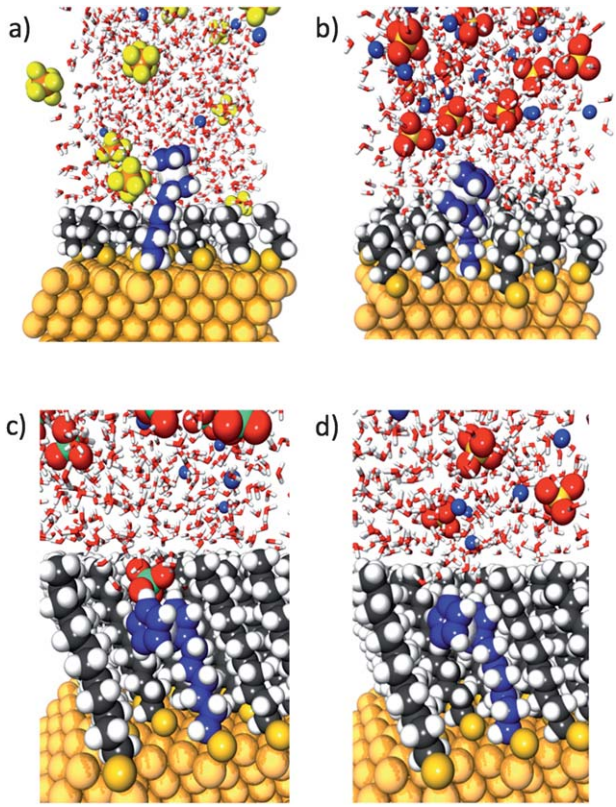

Fig. 3 Typical configurations at $\lambda = 1.0$ of (a) A with PF_6^- (b) A with SO_4^{2-} (c) B with ClO_4^- and (d) B with SO_4^{2-}.

reduced, the anion rather resides on top of the monolayer forming a rigid two-dimensional ionic layer.[12,31,53–55]

3.3 Dehydration

It is now established that the anion solvation directly impacts on the stability of ferrocenium-terminated SAMs.[12,22,30,31] Uosaki *et al.* explained the strongest ion-pair by smaller hydration energy of anions.[13,14] To further investigate this phenomenon, we have first performed simulations of ClO_4^-, PF_6^- and SO_4^{2-} in bulk conditions

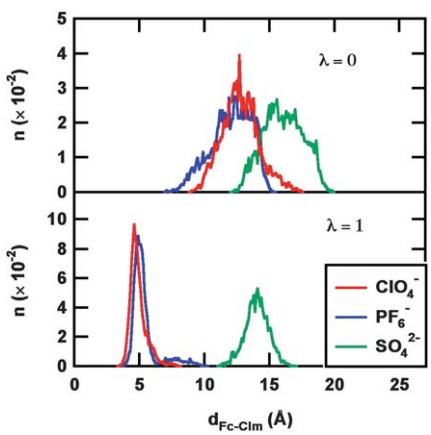

Fig. 4 Distributions of the distance between the ferrocene group and the closest anion in B as a function of the electrolyte anions for $\lambda = 0.0$ and $\lambda = 1.0$.

to estimate their energies of solvation. For PF_6^-, the simulations are predictive due to the lack of experimental properties. The radial distribution functions (RDF) between the anion center of mass and the oxygen atom of water molecules are shown in Fig. 5 We check that the distribution function calculated for ClO_4^- matches very well with that calculated for PF_6^-. We may discern only one hydration shell located at a distance of approximately 4.4 Å for these hydrophobic anions. On the other hand, the RDF for SO_4^{2-} clearly displays two shells and also a significant difference in the height of the first peak. The mean distance between the sulfate anion and the oxygen of water molecule in the second hydration shell is located at 6.6 Å. As a result, the number of water molecules characterizing the hydration of the anions is calculated up to this distance of 6.6 Å. These average hydration numbers, as well as the calculated hydration energies, are reported in Table 4. The values calculated for the perchlorate and sulfate anions agree very well with the corresponding experimental data of Marcus,[56] SO_4^{2-} has a greater hydration energy. This hydrophilic anion is transported with large amounts of solvent, and thus may interact less favorably with the ferrocenium cation. Unlike the sulfate anion, ClO_4^- and PF_6^- can be transported with almost no associated water molecules. They are thus hydrophobic anions that strongly interact with ferrocenium. Obviously, the ability of ion-pairing is well correlated with the sequence of the known hydration energies of the anions. It is thoroughly consistent with various experimental studies.[12,22,30,31]

The thermodynamic cost to be paid for the ion-pair formation is a partial desolvation of anions. This is confirmed in Fig. 6 where the profile of the average number of water molecules is given at each z-position in the initial and final states for each anion. In line with the absence of ion pairing for SO_4^{2-}, we clearly find in Fig. 6 no desolvation of this hydrophilic anion. As a comparison, we see in panels a) and c) a partial dehydration of hydrophobic anions even in the SAMs before oxidation. It is more favorable for these anions to lose water molecules and get favorable interactions with alkyl chains, as expected from their hydrophobic behaviors. For $\lambda = 1.0$, dramatic changes in the number of water molecules of ClO_4^- and PF_6^- are observed, especially in B due to the inclusion of these anions into the layer.

3.4 Energy contributions

We report in Table 5 the electrolyte anion-ferrocenium cation interaction and the electrolyte anion-water molecules interaction as a function of the electrolyte anion in A and B. These calculated values correspond to the difference between $\lambda = 1.0$ and $\lambda = 0.0$.

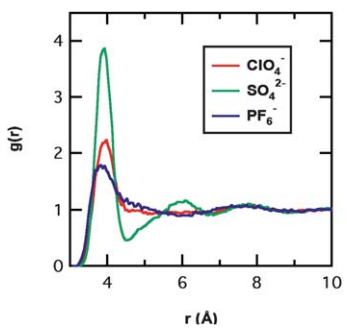

Fig. 5 Computed anions–O_w radial distribution functions in bulk conditions. O_w denotes the oxygen atom of water molecules.

Table 4 Radius of gyration R_g (Å), number of hydration in a 6.6 Å sphere N_{H_2O}, calculated hydration energy E_{hyd}^{calc} (kJ mol^{-1}) and experimental value E_{hyd}^{calc} (kJ mol^{-1}) for the anions in bulk water

	R_g	N_{H_2O}	E_{hyd}^{calc}	E_{hyd}^{calc}
ClO_4^-	1.21	37	−295	−246
PF_6^-	1.43	35	−230	
SO_4^{2-}	1.22	40	−970	−1018

To further analyze these contributions, we report in the same table, the change in the hydration number of the anions with respect to the neutral state. The positive contribution (B-A) change for $\Delta E_{ClO_4^-/H_2O}$ and $\Delta E_{PF_6^-/H_2O}$ is clearly explained at a microscopic level by the stronger desolvation of the hydrophobic anions. We observe that this strong energy change is not compensated by the favorable energy change due to the ion-pair formation. The (B-A) energy contribution between ClO_4^- and FcC_6S is only equal to −29 kJ mol^{-1} whereas it is equal to 154 kJ mol^{-1} for the ClO_4^-/H_2O interaction. We must discuss the enthalpy–entropy compensation to understand the thermodynamic behavior of these systems. Let us recall that the formation of ion pairs in homogeneous systems is enthalpically unfavored and also entropically favored.[57–61] As a result, knowledge of the ΔS properties is required.

It is very difficult to predict and to explain the change in entropy at a microscopic level. However, it is known that desolvation leads to a positive contribution to $T\Delta S$ whereas the formation of ion-pair gives a negative contribution to $T\Delta S$. Moreover, the important loss of degrees of freedom for longer-chain coadsorbates due to the insertion of anions into the film would led to a more negative $T\Delta S$ value in B than in A. To illustrate these considerations, we apply operational expressions for the calculation of the entropy using the TI formalism[42] in

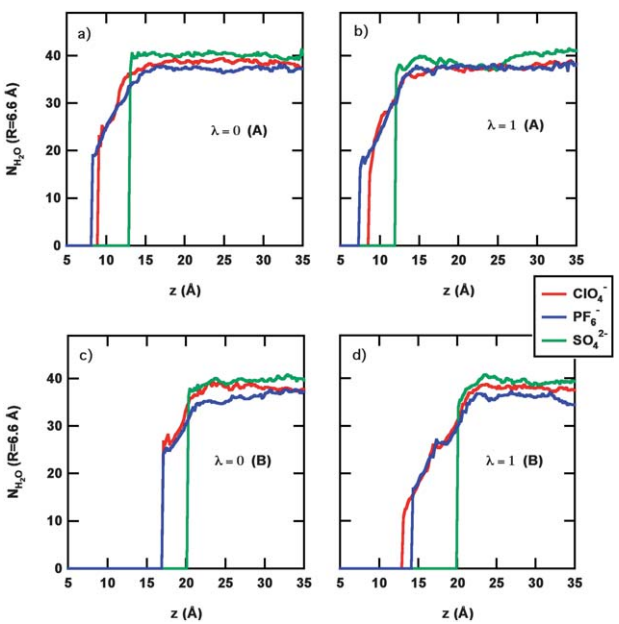

Fig. 6 The profile of the number of water molecules as a function of z for each anion for system A at a) $\lambda = 0.0$, b) $\lambda = 1.0$. The same profiles are given in panels c) $\lambda = 0.0$ and d) $\lambda = 1.0$ for system B. The number of water molecules is calculated by integrating the RDF up to 6.6 Å.

Table 5 Differences of energy contributions (kJ mol^{-1}) and difference in number of water molecules between oxidized and neutral forms in C_{12} and C_4 systems for the different types of electrolyte

		A	B	B-A
ClO_4^-	$\Delta E_{Fc/ClO_4^-}$	−17	−46	−29
	$\Delta E_{ClO_4^-/H_2O}$	−19	135	154
	ΔN_{H_2O}	1	12	11
PF_6^-	$\Delta E_{Fc/PF_6^-}$	−22	−38	−15
	$\Delta E_{PF_6^-/H_2O}$	85	90	5
	ΔN_{H_2O}	6	8	2
SO_4^{2-}	$\Delta E_{Fc/SO_4^{2-}}$	−4	0	4
	$\Delta E_{SO_4^{2-}/H_2O}$	108	15	−93
	ΔN_{H_2O}	2	0	−2

systems involving ion-pairs. The difference in the $T\Delta S$ is calculated from $T\Delta\Delta S = T\Delta S_B - T\Delta S_A$ for ClO_4^- and PF_6^-. The values are reported in Table 6. It can be noticed that the sign of $\Delta\Delta S$ is negative for the two ions. This probably indicates that the major contribution to the entropy change comes from the formation of ion-pairs and the resulting important loss of degrees of freedom. Furthermore, the $T\Delta S$ term is less unfavored for ClO_4^- than for PF_6^-, in line with the stronger desolvation of the perchlorate anion in B as shown in Table 6.

4 Conclusions

The free energy perturbation methods have been applied to predict the shift in the redox potential as the coadsorbed chain length increases from 4 to 12 carbons as a function of the electrolyte anions (*e.g.*, $NaClO_4$, Na_2SO_4, $NaPF_6$). The excellent agreement between the simulated and available experimental redox properties (ClO_4^- and SO_4^{2-}) shows the efficiency of these methods. The free energy perturbation methods is then able to reproduce the small difference in the redox properties as a function of the electrolyte anion. The $\Delta\Delta G^{cal}_{redox}$ values increase in the following order: $ClO_4^- < PF_6^- < SO_4^{2-}$. The $\Delta\Delta G$ is relevant to conclude the stability of the environment upon oxidation because it involves the sum of all the energy contributions.

From the investigation of the density profiles of the different species along the normal to the surface, we have shown the poorest ion-pairing ability of SO_4^{2-}. The formation of strong surface ion-pairs that stabilize the electrogenerated cations for $NaClO_4$ and $NaPF_6$ is established from our simulations. Actually, MD simulations clearly show that the ion-pair is stronger in FcC_6S–/$C_{12}S$–Au (B) than in FcC_6S–/C_4S–Au (A). The formation of the ion-pair is more favored for monolayer systems with longer alkyl chains, as the environment of the ferrocenium becomes more alkane-like. The results indicate that the flexibility of the film is strongly reduced in B due to the deep insertion of the anions into the film to form tightly ions-pairs to the ferroceniums.

Table 6 Differences for the oxidation process in Gibbs free energy variations, enthalpy variations and entropy variations (kJ mol^{-1}). The number of water molecules lost in the hydration sphere ($\Delta\Delta N_{H_2O}$) between system A and system B for ClO_4^- and PF_6^- anions is given for comparison

	$\Delta\Delta G$	$\Delta\Delta H$	$T\Delta\Delta S$	$\Delta\Delta N_{H_2O}$
ClO_4^-	21	14	−7	11
PF_6^-	23	9	−14	2

The ability of ion-pairing correlates with the sequence of the known hydration energies of the anions. SO_4^{2-} is transported with large amounts of solvent, and thus may interact less with the ferrocenium cation, unlike ClO_4^- and PF_6^- that can be transported with almost no associated water.

We have completed this work by an investigation of the desolvation of the anions for the strongly associating ClO_4^- and PF_6^-. After the oxidation of the ferrocene group, dramatic changes in the number of water molecules of ClO_4^- and PF_6^- are observed, especially in B. This stronger desolvation gives a positive contribution change between the electrolyte hydrophobic anion and the water molecules that is not compensated by the favorable energy change. This analysis establishes that the ion-pair formation should be analyzed in the context of the enthalpy–entropy compensation effect.

5 Appendix: Computational details

Table 7 Partial charges for the atoms involved in the perturbation process and Lennard-Jones parameters for the sodium cation in the initial ($\lambda = 0.0$) and final state ($\lambda = 1.0$) in the A and B systems

Parameters	initial state $\lambda = 0.0$	Final state $\lambda = 1.0$
CA		
q (e)	−0.1	−0.04433
HA		
q (e)	0.09	0.14040
Fe		
q (e)	0.10	0.17970
CT		
q (e)	−0.090	−0.120
HC		
q (e)	0.060	0.060
Na		
q (e)	1.0	0.0
σ (Å)	3.3304	0.0
ε (kJ mol^{-1})	0.01161	0.0

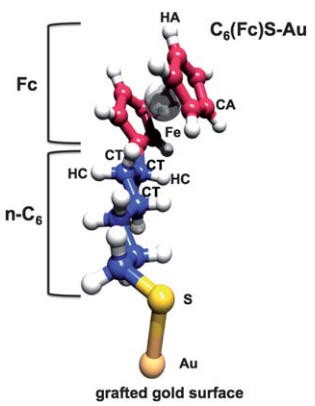

Fig. 7 Labeling scheme of the ferrocenylhexanethiolate chain (FcC_6S–Au) used in this work. The partial charges of the different atom types between the reduced and oxidized states are given in Table 7.

6 Acknowledgments

This work was granted access to the HPC resources of IDRIS under the allocation 2011-i2010092119 made by GENCI (Grand Equipement National de Calcul Intensif).

References

1 C. E. D. Chidsey, *Science*, 1991, **251**, 919.
2 C. E. D. Chidsey, C. R. Bertozzi, T. M. Putwinski and A. M. Mujsce, *J. Am. Chem. Soc.*, 1990, **112**, 4301.
3 S. E. Creager and G. K. Rowe, *Anal. Chim. Acta*, 1991, **246**, 233.
4 S. E. Creager and G. K. Rowe, *J. Electroanal. Chem.*, 1994, **370**, 203.
5 J. F. Smalley, S. W. Feldberg, C. E. D. Chidsey, M. R. Linford, M. D. Newton and Y.-P. Liu, *J. Phys. Chem.*, 1995, **99**, 13141.
6 K. Weber, L. Hockett and S. Creager, *J. Phys. Chem. B*, 1997, **101**, 8286.
7 J. J. Sumner, K. S. Weber, L. A. Hockett and S. E. Creager, *J. Phys. Chem. B*, 2000, **104**, 7449.
8 F. Quist, V. Tabard-Cossa and A. Badia, *J. Phys. Chem. B*, 2003, **107**, 10691–10695.
9 L. L. Norman and A. Badia, *J. Am. Chem. Soc.*, 2009, **131**, 2328.
10 M. Y. Ho, P. Li, P. Estrela, S. Goodchild and P. Migliorato, *J. Phys. Chem. B*, 2010, **114**, 10661–10665.
11 L. Muller-Meskamp, S. Karthauser, R. Waser, M. Homberger, Y. Wang, U. Englert and U. Simon, *Surf. Sci.*, 2009, **603**, 716–722.
12 L. L. Norman and A. Badia, *J. Phys. Chem. C*, 2011, **115**, 1985–1995.
13 K. Uosaki, Y. Sato and H. Kita, *Electrochim. Acta*, 1991, **7**, 1793.
14 K. Uosaki, Y. Sato and H. Kita, *Langmuir*, 1991, **7**, 1510.
15 S. E. Creager and G. K. Rowe, *J. Electroanal. Chem.*, 1997, **420**, 291–299.
16 L. Y. S. Lee, T. C. Sutherland, S. Rucareanu and R. B. Lennox, *Langmuir*, 2006, **22**, 4438.
17 X. Yao, J. Wang, F. Zhou, J. Wang and N. Tao, *J. Phys. Chem. B*, 2004, **108**, 7206.
18 S. Ye, Y. Sato and K. Uosaki, *Langmuir*, 1997, **13**, 3157.
19 Y. Guo, J. Zhao and J. Zhu, *Thin Solid Films*, 2008, **516**, 3051.
20 G. K. Rowe and S. E. Creager, *J. Phys. Chem.*, 1994, **98**, 5500–5507.
21 G. K. Rowe and S. E. Creager, *Langmuir*, 1994, **10**, 1186.
22 G. K. Rowe and S. E. Creager, *Langmuir*, 1991, **7**, 2307.
23 D. M. Collard and M. A. Fox, *Langmuir*, 1991, **7**, 1192.
24 D. Buttry, *Langmuir*, 1990, **6**, 1319.
25 F. Goujon, C. Bonal, B. Limoges and P. Malfreyt, *Langmuir*, 2009, **25**, 9164.
26 F. Goujon, C. Bonal and P. Malfreyt, *Mol. Simul.*, 2009, **35**, 538–546.
27 F. Goujon, C. Bonal, B. Limoges and P. Malfreyt, *Mol. Phys.*, 2008, **106**, 1397.
28 F. Goujon, C. Bonal, B. Limoges and P. Malfreyt, *J. Phys. Chem. B*, 2010, **114**, 6447–6454.
29 G. Filippini, F. Goujon, C. Bonal and P. Malfreyt, *J. Phys. Chem. B*, 2010, **114**, 12897–12907.
30 H. X. Ju and D. Leech, *Phys. Chem. Chem. Phys.*, 1999, **1**, 1549.
31 G. Valincius, G. Niaura, B. Kazakevicienė, Z. Talaikyté, M. Kazamékaité, E. Butkus and V. Razumas, *Langmuir*, 2004, **20**, 6631.
32 W. D. Cornell, P. Cieplak, C. I. Bayly, I. R. Gould, K. J. Merz, D. M. Ferguson, D. M. Spellmeyer, T. Fox, J. W. Caldwell and P. Kollman, *J. Am. Chem. Soc.*, 1995, **117**, 5179.
33 J. P. Ryckaert, G. Cicotti and H. J. C. Berendsen, *J. Comput. Phys.*, 1977, **23**, 327.
34 J. L. F. Abascal and C. Vega, *J. Chem. Phys.*, 2005, **123**, 234505.
35 J. Aqvist, *J. Phys. Chem.*, 1990, **94**, 8021.
36 M. Klähn, A. Seduraman and P. Wu, *J. Phys. Chem. B*, 2008, **112**, 10989.
37 G. A. Kaminski and W. L. Jorgensen, *J. Chem. Soc., Perkin Trans.*, 1999, **2**, 2365–2375.
38 W. R. Cannon, B. M. Pettit and J. A. McCammon, *J. Phys. Chem.*, 1994, **98**, 6225–6230.
39 U. Essmann, L. Perera, M. L. Berkowitch, T. Darden, H. Lee and L. G. Pedersen, *J. Chem. Phys.*, 1995, **98103**, 8577.
40 I.-C. Yeh and M. L. Berkowitz, *J. Chem. Phys.*, 1999, **111**, 3155.
41 E. R. Smith, *Proc. R. Soc. London, Ser. A*, 1981, **375**, 475.
42 A. Ghoufi and P. Malfreyt, *Mol. Phys.*, 2006, **104**, 2929–2943.
43 W. G. Hoover, *Phys. Rev. A: At., Mol., Opt. Phys.*, 1985, **31**, 1695.
44 DL_POLY is a parallel molecular dynamics simulation package developed at the Daresbury Laboratory Project for Computer Simulations under the auspices of the EPSRC for the Collaborative Computational Project for Computer Simulation of Condensed Phases (CCP5) and the Advanced Research Computing Group (ARCG) at the Daresbury Laboratory.
45 J. N. C. Lopes, P. C. do Couto and M. E. M. da Piedade, *J. Phys. Chem. A*, 2006, **110**, 13850.
46 P. Honenberg and W. Kohn, *Phys. Rev.*, 1964, **136**, 864.
47 W. Kohn and L. Sham, *Phys. Rev.*, 1965, **140**, 1133.
48 A. D. Becke, *Phys. Rev. A: At., Mol., Opt. Phys.*, 1988, **38**, 3098.
49 A. D. Becke, *J. Chem. Phys.*, 1993, **98**, 5648.
50 J. P. Perdew and Y. Wang, *Phys. Rev. E*, 1991, **45**, 13244.
51 M. J. Frisch, G. W. Trucks, H. B. Schelgel, G. E. Scuseria, M. A. Robb, J. R. Cheesemann, J. A. Montgomery, J. Vreven, K. N. Kudin, J. C. Burant, J. M. Millam, S. S. Iyengar, J. Tomasi, V. Barone, B. Mennucci, M. Cossi, G. Scalmani, N. Rega, G. A. Petersson, T. Nakajima, Y. Honda, O. Kitao, H. Nakai, M. Klene, X. Li, J. E. Knox, H. P. Hratchian, J. B. Cross, V. Bakken, C. Adamo, J. Jaramillo, R. Gomperts, R. E. Stratmann, O. Yazyev, A. J. Austin, R. Cammi, C. Pomelli, J. W. Ochterski, P. Y. Ayala, K. Morokuma, G. A. Voth, P. Salvador, J. J. Dannenberg, V. G. Zakrzewski, S. Dapprich, A. D. Daniels, M. C. Strain, O. Farkas, D. K. Malick, A. D. Rabuck, K. Raghavachari, J. B. Foresman, J. V. Ortiz, Q. Cui, A. G. Baboul, S. Clifford, J. Ciolkowski, B. B. Stefanov, G. Liu, A. Liashenko, P. Piskorz, I. Komaromi, R. L. Martin, D. J. Fox, T. Keith, M. A. Al-Laham, C. Y. Peng, A. Nanayakkara, M. Challacombe, P. M. W. Gill, B. Johnson, W. Chen, M. W. Wong, C. Gonzalez and J. A. Pople, Gaussian, Inc., Wallingford CT, 2004.
52 C. P. Breneman and K. B. Wiberg, *J. Comput. Chem.*, 1990, **11**, 361.
53 K. Shimazu, I. Yagi, Y. sato and K. Uosaki, *J. Electroanal. Chem.*, 1994, **372**, 117.
54 B. Kazakevicien, G. Valincius, G. Niaura, Z. Talaikyt, M. Kaemkait, V. Razumas, D. Plauinatis, A. Teierskien and V. Lisauskas, *Langmuir*, 2007, **23**, 4965.
55 L. Norman and A. Badia, *Langmuir*, 2007, **23**, 10198.
56 Y. Marcus, *J. Chem. Soc., Faraday Trans. 1*, 1987, **83**, 339–349.
57 C. Bonal, Y. Israëli, J.-P. Morel and N. Morel-Desrosiers, *J. Chem. Soc., Perkin Trans. 2*, 2001, (7), 1075.
58 A. Mendes, C. Bonal, N. Morel-Desrosiers, J. P. Morel and P. Malfreyt, *J. Phys. Chem. B*, 2002, **106**, 4516.
59 A. Ghoufi, C. Bonal, J.-P. Morel, N. Morel-Desrosiers and P. Malfreyt, *J. Phys. Chem. B*, 2004, **108**, 11744.
60 A. Ghoufi, C. Bonal, J.-P. Morel, N. Morel-Desrosiers and P. Malfreyt, *J. Phys. Chem. B*, 2004, **108**, 5095.
61 B. E. Conway, *Comprehensive Treatise of Electrochemistry*, Plenum Press, New York, 1983, vol. 5.

